ELSEVIER

Advances in Water Resources 25 (2002) 1215–1231

Advances in Water Resources

www.elsevier.com/locate/advwatres

An overview of research on Eulerian–Lagrangian localized adjoint methods (ELLAM)

Thomas F. Russell [a,*], Michael A. Celia [b]

[a] Department of Mathematics, University of Colorado at Denver, Denver, CO 80217-3364, USA
[b] Department of Civil and Environmental Engineering, Princeton University, Princeton, NJ 08544, USA

Received 29 January 2002; received in revised form 28 February 2002; accepted 10 March 2002

Abstract

For problems of convection–diffusion type, Eulerian–Lagrangian localized adjoint methods provide a methodology that maintains the accuracy and efficiency of Eulerian–Lagrangian methods, while also conserving mass and systematically treating any type of boundary condition. In groundwater hydrology, this framework is useful for solute transport, as well as vadose-zone transport, multiphase transport, and reactive flows. The formulation was originated around 1990 by the authors, Herrera and Ewing, in a paper that appeared in Advances in Water Resources [Adv. Water Resour. 13 (1990) 187]. This paper reviews the progress in the development, analysis, and application of these methods since 1990, and suggests topics for future work.

1. Introduction

The Eulerian–Lagrangian localized adjoint method (ELLAM) was developed about 10 years ago, with the first journal publication appearing in Advances in Water Resources in 1990. Since that time, the method has been expanded and modified in a number of important ways. Today, the method can be applied to many practical problems, and continues to undergo development to address new and more complex applications.

ELLAM is an attractive numerical approach for solution of contaminant transport problems because it is general, it is based on a sound theoretical foundation, it uses a characteristic framework in which approximating equations are written, and mass conservation is an inherent property of the method. The approach is based on test functions that are defined as solutions to the formal adjoint operator defined on local space-time partitions of the domain. The initial journal publication [11] appeared in Advances in Water Resources, and dealt with a simple one-dimensional, constant-coefficient, transient advection–diffusion equation. Celia et al. showed both the superior numerical performance, and the mass-conservation properties of the method. Since that publication, the ELLAM has been developed for, and applied to, a number of more complex problems, including two- and three-dimensional advection–diffusion–reaction equations (see, for example, [7,27,55,60]). In all of these cases, ELLAM performs well because it combines a Lagrangian approach for the advective terms with appropriate approximations, consistent with the Lagrangian framework, for other terms in the equations. Such an approach often produces effective and robust numerical methods for complex transport equations.

In the present paper, we present a general overview and review of the ELLAM approach for solution of contaminant transport equations. We begin with a presentation of the ELLAM framework, in which the salient features of the method are presented for a one-dimensional advection–diffusion–reaction equation. We choose a relatively simple example in order to demonstrate the basic features of the method in a simple setting. This presentation is followed by a discussion of how ELLAM has been extended for application to practical problems. Extensions include two and three spatial dimensions, nonconstant coefficients, nonlinearities, and details of tracking algorithms. Following this, we survey application areas for which ELLAM has been applied, choosing a few example solutions to demonstrate the kinds of problems that have been solved. Finally, we provide a few brief comments on other

* Corresponding author. Tel.: +1-303-556-4813; fax: +1-303-556-8550.
E-mail address: trussell@carbon.cudenver.edu (T.F. Russell).

0309-1708/02/$ - see front matter
PII: S0309-1708(02)00104-5

Eulerian–Lagrangian methods used to solve transport equations, discuss how these methods relate to the ELLAM framework, and conclude with suggestions of topics for future research.

2. The ELLAM framework

To describe the general ideas that underlie the ELLAM approach, a simple one-dimensional advection–diffusion–reaction equation will be approximated using the method. This allows the important steps in the procedure to be highlighted and described in a simple setting. Once the framework is completed for this case, a variety of extensions will be presented to allow practical applications to be solved.

To develop the ELLAM framework, the following advection–diffusion–reaction equation in one space dimension will be used as a model:

$$R\frac{\partial u}{\partial t}+V\frac{\partial u}{\partial x}-D\frac{\partial^2 u}{\partial x^2}+\lambda u=f(x,t),\quad 0<x<L,\ \ t>0. \tag{1}$$

For simplicity, assume that the coefficients are constants. The ELLAM idea uses general concepts of localized adjoint methods [28,29] to define test functions based on specific solutions to the homogeneous adjoint equation associated with the governing equation (1). Test functions for ELLAM use space-time formulations such that solutions are sought to the following weak form of the governing equation:

$$\int_{\Omega_t}\int_{\Omega_x}\left(R\frac{\partial u}{\partial t}+V\frac{\partial u}{\partial x}-D\frac{\partial^2 u}{\partial x^2}+\lambda u\right)w(x,t)\,\mathrm{d}x\,\mathrm{d}t = \int_{\Omega_t}\int_{\Omega_x} f(x,t)w(x,t)\,\mathrm{d}x\,\mathrm{d}t. \tag{2}$$

Integration by parts in both space and time yields the adjoint operator, and the test function is chosen to satisfy the homogeneous version of the adjoint equation,

$$-R\frac{\partial w}{\partial t}-V\frac{\partial w}{\partial x}-D\frac{\partial^2 w}{\partial x^2}+\lambda w=0. \tag{3}$$

The ELLAM approximation results from a specific solution to this equation, based on an operator splitting approach, such that w is required to satisfy the following equations:

$$\begin{aligned} &-R\frac{\partial w}{\partial t}-V\frac{\partial w}{\partial x}+\lambda w=0,\\ &D\frac{\partial^2 w}{\partial x^2}=0. \end{aligned} \tag{4}$$

The function satisfying Eq. (4) is linear in x while varying exponentially along the characteristic directions given by

$$\frac{\mathrm{d}x}{\mathrm{d}t}=\frac{V}{R}. \tag{5}$$

Discrete approximations require discretization of the spatial and temporal domains with subsequent application of the ELLAM ideas in this discretized system. Let the spatial domain be discretized using N discrete points (nodes), separated by distances $\Delta x_i = x_{i+1}-x_i$, $i=1,2,\ldots,N-1$. Let the time domain be discretized using discrete time levels t^n separated by $\Delta t^n = t^{n+1}-t^n$, $n=0,1,2,\ldots$ In this discrete system, time-stepping from one time level to the next (t^n to t^{n+1}) requires N equations for the N unknowns at the new time level. To construct these equations, one ELLAM test function is associated with each of the nodal points i at the new time level t^{n+1}. This test function is denoted by $w_i^{n+1}(x,t)$. The ELLAM procedure defines test functions that satisfy Eqs. (4) piecewise, on a space-time grid that is consistent with the characteristic directions of Eq. (5). One standard choice is the usual piecewise-linear function defined with respect to the spatial grid points at time t^{n+1}, tracking along the relevant characteristics to time t^n, and modified for the exponential behavior due to the reaction term in the equation:

$$w_i^{n+1}(x,t)=\begin{cases} \left(\frac{x^*-x_{i-1}^*}{\Delta x_{i-1}}\right)\exp\left[\frac{\lambda}{R}(t-t^n)\right], \\ \quad x_{i-1}^*\leqslant x^*\leqslant x_i^*, t^n<t<t^{n+1}, \\ \left(\frac{x_{i+1}^*-x^*}{\Delta x_i}\right)\exp\left[\frac{\lambda}{R}(t-t^n)\right], \\ \quad x_i^*\leqslant x^*\leqslant x_{i+1}^*, t^n<t<t^{n+1}, \\ 0, \quad \text{all other } x^*,t, \end{cases} \tag{6}$$

where

$$x^*\equiv x-\frac{V}{R}\left(t^{n+1}-t\right). \tag{7}$$

This function is shown schematically in Fig. 1, for the case of $\lambda=0$. The ELLAM equations on the discretized domain then take the form

$$\int_{\Omega_t}\int_{\Omega_x}\left(R\frac{\partial u}{\partial t}+V\frac{\partial u}{\partial x}-D\frac{\partial^2 u}{\partial x^2}+\lambda u\right)w_i^{n+1}(x,t)\,\mathrm{d}x\,\mathrm{d}t = \int_{\Omega_t}\int_{\Omega_x} f(x,t)w_i^{n+1}(x,t)\,\mathrm{d}x\,\mathrm{d}t. \tag{8}$$

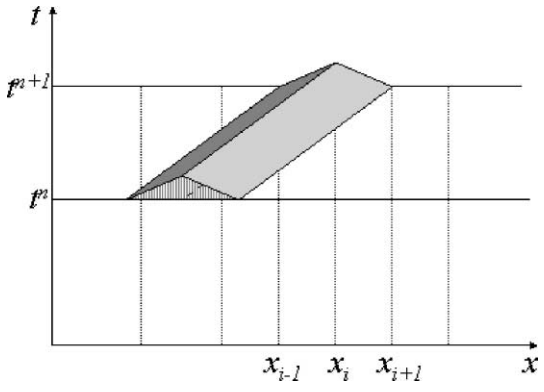

Fig. 1. One-dimensional ELLAM test function.

Integration by parts, and imposition of the constraints of Eq. (4), lead to the following ELLAM equation:

$$\int_{\Omega_x} Ru(x,t^{n+1})w_i^{n+1}(x,t^{n+1})\,\mathrm{d}x - \int_{\Omega_x} Ru(x,t^n)w_i^{n+1}(x,t^n)\,\mathrm{d}x + D\int_{t^n}^{t^{n+1}}\int_{\Omega_x}\frac{\partial u}{\partial x}\frac{\partial w_i^{n+1}}{\partial x}\,\mathrm{d}x\,\mathrm{d}t = \int_{\Omega_t}\int_{\Omega_x} f(x,t)w_i^{n+1}(x,t)\,\mathrm{d}x\,\mathrm{d}t, \tag{9}$$

where the test function $w_i^{n+1}(x,t)$ is assumed to remain in the interior of the spatial domain, such that it is zero at both the left and right boundaries for all times between t^n and t^{n+1}.

2.1. Boundary conditions

One of the major advantages of ELLAM is the ability to incorporate boundary conditions into the approximating equations with no change in the overall approach. Boundary terms arise naturally in the ELLAM formulation, and these terms allow specified boundary conditions to be imposed directly. The ELLAM boundary terms are a result of nonzero values of test functions intersecting the spatial boundaries of the domain. Consider, for example, the case of the 2-D test function $w_i^{n+1}(x,t)$ shown in Fig. 2 intersecting the inflow boundary ($x=0$). When the analogue of this occurs in 1-D, integration by parts applied to Eq. (8) leads to the following expression:

$$\int_{\Omega_x} Ru(x,t^{n+1})w_i^{n+1}(x,t^{n+1})\,\mathrm{d}x - \int_{\Omega_x} Ru(x,t^n)w_i^{n+1}(x,t^n)\,\mathrm{d}x + D\int_{t^n}^{t^{n+1}}\int_{\Omega_x}\frac{\partial u}{\partial x}\frac{\partial w_i^{n+1}}{\partial x}\,\mathrm{d}x\,\mathrm{d}t - \int_{t^n}^{t^{n+1}}\left[Vu(0,t) - D\frac{\partial u}{\partial x}(0,t)\right]w_i^{n+1}(0,t)\,\mathrm{d}t = \int_{\Omega_t}\int_{\Omega_x} f(x,t)w_i^{n+1}(x,t)\,\mathrm{d}x\,\mathrm{d}t. \tag{10}$$

In this case, the boundary integral at $x=0$ accounts for mass entering the domain through the boundary, with that mass reaching the location within the domain where the test function $w_i^{n+1}(x,t^{n+1})$ is nonzero. This mass is then accounted for in the equation associated with test function w_i^{n+1}.

Outflow boundaries are treated in a similar way. A boundary integral will appear in any ELLAM equation for which the test function is nonzero along any part of the outflow boundary, between times t^n and t^{n+1}. If the outflow boundary is assumed to be the point $x=L$, then the function $w_N^{n+1}(x,t)$ is the only test function that is nonzero at $x=L$. If this test function is defined such that it is equal to one at all spatial points between $x_N^*(t^n)$ and x_N, at time t^n, and it follows the same exponential behavior as all other test functions, then an additional boundary term arises along the outflow boundary for the equation associated with $w_N^{n+1}(x,t)$. That term takes the form

$$\int_{t^n}^{t^{n+1}}\left[Vu(L,t) - D\frac{\partial u}{\partial x}(L,t)\right]w_N^{n+1}(L,t)\,\mathrm{d}t. \tag{11}$$

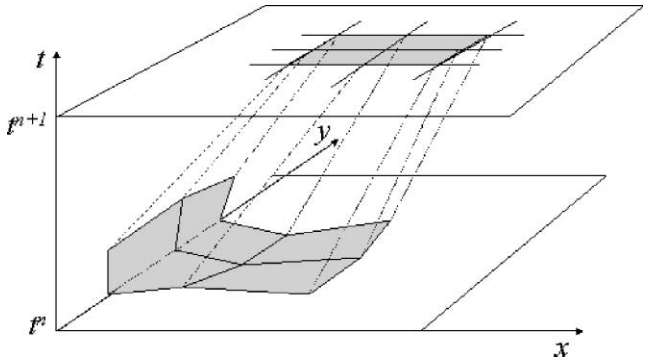

Fig. 2. Nonzero support of a two-dimensional test function that intersects the inflow boundary.

Given the boundary contributions at both the inflow and outflow boundaries, a general expression for the discrete ELLAM equations may be obtained by combination of Eqs. (9)–(11), which leads to the following equation:

$$\int_{\Omega_x} Ru(x,t^{n+1})w_i^{n+1}(x,t^{n+1})\,\mathrm{d}x - \int_{\Omega_x} Ru(x,t^n)w_i^{n+1}(x,t^n)\,\mathrm{d}x + D\int_{t^n}^{t^{n+1}}\int_{\Omega_x}\frac{\partial u}{\partial x}\frac{\partial w_i^{n+1}}{\partial x}\,\mathrm{d}x\,\mathrm{d}t + \int_{t^n}^{t^{n+1}}\left\{\left[Vu(x,t) - D\frac{\partial u}{\partial x}(x,t)\right]w_i^{n+1}(x,t)\right\}\Big|_{x=0}^{x=L}\mathrm{d}t = \int_{\Omega_t}\int_{\Omega_x} f(x,t)w_i^{n+1}(x,t)\,\mathrm{d}x\,\mathrm{d}t. \tag{12}$$

2.2. Conservation of mass

The natural inclusion of all types of boundary conditions in the ELLAM equations leads to a second advantage of the method, namely global mass conservation. This is true for both the nonreactive and the reactive forms of the governing equation. Global conservation can be shown easily by summation of all equations, meaning summation of Eq. (12) over all i $(i=1,2,\ldots,N)$. Given that $\sum_{i=1}^{N} w_i^{n+1}(x,t) = \exp[(\lambda/R)(t-t^n)]$, the resulting summed equations take the form

$$\left(\exp\left[\frac{\lambda\Delta t^n}{R}\right]\right)\int_{\Omega_x} Ru(x,t^{n+1})\,\mathrm{d}x - \int_{\Omega_x} Ru(x,t^n)\,\mathrm{d}x + \int_{t^n}^{t^{n+1}}\left\{\left[Vu(x,t) - D\frac{\partial u}{\partial x}(x,t)\right]\exp\left[\frac{\lambda}{R}(t-t^n)\right]\right\}\Bigg|_{x=0}^{x=L}\mathrm{d}t = \int_{t^n}^{t^{n+1}}\int_{\Omega_x} f(x,t)\exp\left[\frac{\lambda}{R}(t-t^n)\right]\mathrm{d}x\,\mathrm{d}t. \tag{13}$$

This equation can be seen as a discrete (in time) version of the mass conservation statement that results from integration of Eq. (1) over the spatial domain, and between times t^n and t^{n+1}.

While the ELLAM equations provide demonstrable global mass conservation, the equations based on test functions of Eq. (6) fail to conserve mass locally. If local mass conservation is desired, then an alternative choice for test functions, which still satisfies the constraints of Eq. (4), may be defined as follows:

$$w_i^{n+1}(x,t) = \begin{cases} \exp\left[\frac{\lambda}{R}(t-t^n)\right], \\ \quad x_{i-1}^* \leqslant x^* \leqslant x_i^*,\ t^n < t < t^{n+1}, \\ 0, \quad \text{all other } x^*, t, \end{cases} \tag{14}$$

where x^* is again as in (7). Eq. (12) remains as the ELLAM expression for this new set of test functions, with appropriate treatment of the derivatives in the diffusion integral. The global mass balance statement of Eq. (13) also continues to hold, because the summation of test functions is the same for both sets of functions. The difference is in local mass conservation, where the local expression (Eq. (12)) now also corresponds to a statement of (local) mass conservation.

ELLAM schemes based on the test functions of Eq. (6) are referred to as finite-element ELLAM (FE-ELLAM) approximations, while those associated with the test functions of Eq. (14) are referred to as finite-volume ELLAM (FV-ELLAM) approximations.

2.3. Evaluation of integrals

The general ELLAM approximation equation has five general integrals: (1) the spatial integral at the new time level, (2) the spatial integral at the old time level, (3) the integral along the inflow boundary, (4) the integral along the outflow boundary and (5) the integral involving the source/sink term. In order to evaluate these integrals, specific functional forms must be chosen to represent the unknown $u(x,t)$. To be consistent with the discretization that has already been defined, a trial function may be introduced using standard piecewise polynomials,

$$u(x,t) \approx \hat{u}(x,t) = \sum_{j=1}^{N} U_j(t)\phi_j(x). \tag{15}$$

In this equation, the coefficients U_j represent nodal unknowns, defined on the fixed grid, and the ϕ_j are interpolation functions, typically taken to be piecewise-linear Lagrange polynomials (chapeau functions). With this interpolation defined, the different integrals may be evaluated. The first integral is calculated by substitution of the trial function into the integrand, such that

$$\int_{\Omega_x} Ru(x,t^{n+1})w_i^{n+1}(x,t^{n+1})\,\mathrm{d}x \approx R\sum_{j=1}^{N} U_j(t)\int_0^L \phi_j(x)w_i^{n+1}(x,t^{n+1})\,\mathrm{d}x. \tag{16}$$

For piecewise-linear functions (both $\phi_j(x)$ and $w_i^{n+1}(x,t^{n+1})$), this yields standard finite element spatial weights $(1/6, 2/3, 1/6)$ for the unknowns at the new time level. For the finite-volume ELLAM, the weights are $(1/8, 3/4, 1/8)$. Lumping or other procedures may be applied to these terms, depending on the system being modeled and the needs of the application.

The second integral is somewhat more complicated, because the test function has been translated from t^{n+1} to t^n, and therefore is no longer aligned with the spatial grid points (unless, in this case, the Courant number is an integer). For the simple case of one spatial dimension, and constant coefficients, this term can be evaluated analytically. To do so, the test functions are defined explicitly at time t^n, and the resulting product of piecewise-linear functions is evaluated. Results for this case are given in [12]. Because this analytical treatment cannot be used for more complex problems, a second option should also be considered. This involves numerical integration of the form

$$\int_{\Omega_x} Ru(x,t^n)w_i^{n+1}(x,t^n)\,\mathrm{d}x \approx \sum_{p=1}^{NP} W_p\left[R\hat{u}(x_p,t^n)\right]w_i^{n+1}(x_p,t^n). \tag{17}$$

In this equation, p denotes integration points, W_p are integration weighting factors, x_p is the location of the integration point, and NP is the total number of integration points. In Eq. (17), evaluation of the test function at the spatial integration point, at the old time level, means that the test function has to be tracked back in time from t^{n+1} to t^n (define integration points $\tilde{x}_p$ at time t^{n+1}; backtrack to find $x_p = (\tilde{x}_p)^*$ at t^n; then $w_i^{n+1}(x_p,t^n)$ in (17) is determined from (6) or (14) at $(\tilde{x}_p, t^{n+1})$, and $\hat{u}(x_p,t^n)$ is determined from (15) by interpolation at (x_p,t^n)). An alternative is to forward-track the integration points, then evaluate the test function at time t^{n+1} (define integration points x_p at time t^n; forward track to find $\tilde{x}_p$ at t^{n+1} such that $(\tilde{x}_p)^* = x_p$; then $w_i^{n+1}(x_p,t^n)$ is determined from (6) or (14) by interpolation at $(\tilde{x}_p, t^{n+1})$, and $\widehat{u}(x_p,t^n)$ is determined from (15) at (x_p,t^n)) [48]. An advantage of this approach is that, because the test function is defined with respect to the spatial grid at the new time level, its evaluation is easy. This is true with or without the exponential behavior associated with reaction terms. With backtracking, the test function is

defined at (in general) irregularly located points (x_p, t^n), and its interpolation to the spatial domain at t^n is not obvious. While numerical integration is not really necessary for this simplified example (because the integrals can be evaluated analytically, and tracking of test functions is easy), it will become important in cases of multiple spatial dimensions, as discussed in the next section. Also, notice that Eqs. (16) and (17) apply to both the FE-ELLAM and the FV-ELLAM.

Accurate numerical integration of this second integral is important to local and global mass conservation, and to the qualitative appearance of the numerical solution. For global conservation, consider Eq. (13), which corresponds to the summed test function $w^{n+1}(x, t^n) \equiv 1$ at the old time level. For global conservation to hold numerically, the second term must be evaluated exactly. This is straightforward with forward tracking of integration points, because they are defined in a regular fashion at t^n, but is difficult or impossible with backtracking in a variable velocity field. With forward tracking, the mass associated with each integration point is distributed after tracking to the right-hand sides of the discrete equations, in accordance with the values of the corresponding test functions, which sum to 1. The potential difficulties lie in the accurate distribution of the mass (local conservation); if a cell at t^{n+1} receives a disproportionate share of the forward-tracked integration points, it can gain an excess of mass, resulting in spurious oscillations in the numerical solution. This problem is particularly acute with the discontinuous FV-ELLAM test functions of (14), so that FV-ELLAM implementations have smoothed these discontinuities to some extent in order to mitigate this sensitivity [6,7,23,27]. One way to understand this problem is to take $u(x, t^n) \equiv 1$ in (17); poor distribution of mass then corresponds to errors in the integration of $w_i^{n+1}(x, t^n)$. This integration is generally inexact with forward tracking due to interpolation, while with backtracking it will be exact. There is thus a tradeoff between the advantages/disadvantages of backtracking (preserves flat solutions, does not conserve mass, test-function evaluation at t^n difficult) and forward tracking (oscillations, conserves mass, easy test-function evaluation). Recent implementations have favored forward tracking, with modifications to avoid oscillations.

The third integral is associated with inflow boundaries. Again, analytical evaluations can be used for this simple case, but numerical integration can also be defined. The approach for this integral is analogous to that for the spatial integral at the old time level. However, treatment of the boundary integral depends on the type of boundary condition specified. Because physically realistic boundary conditions at inflow boundaries are either fixed concentration or fixed total flux, each of these will be considered in turn, beginning with the total-flux condition. Because the integrand involves the total flux, specification of the total flux means that the boundary integral can be evaluated directly once the test function is defined. Backtracking the test function allows for analytical evaluation of this integral; otherwise numerical integration (now performed in time rather than space) can be defined. In either case, all information in the integrand is known, so the results of the integration are added to the right side of the equation. When the boundary condition is a fixed concentration, only part of the integrand is known (the advective flux), while the diffusive flux is unknown. In this case, the integral is split, with the known part taken to the right side of the equation, and the unknown diffusive flux remaining on the left side of the equation. In early versions of ELLAM, the diffusive flux at the boundary was calculated as an unknown (see, for example, [11]). This adds an extra discrete unknown ($\partial U_1/\partial x$), and causes some difficulties in terms of matrix structure. Another option is to approximate the diffusive flux by forward-tracking the boundary values to the new time level, then using a discrete approximation for $\partial u/\partial x$ at t^{n+1}, written in terms of the nodal unknowns at the new time level, $\{U_j(t^{n+1})\}$. This preserves matrix structure, although it introduces an asymmetry into the matrix.

The fourth integral is the boundary integral along the outflow boundary. While ELLAM can accommodate any type of boundary conditions, for outflow boundaries the usual specification is zero diffusive flux. For simplicity of presentation, we consider only this condition. When the diffusive flux is specified as zero, the diffusive part of the boundary integral is zero, and therefore only the advective part needs to be evaluated. The boundary integral requires knowledge of the function u along the outflow boundary, between times t^n and t^{n+1}. One option is to define the function as a linear combination of $U_N(t^n)$ and $U_N(t^{n+1})$, along the time axis. Then the outflow integral, which applies to the equation associated with node N, becomes

$$\int_{t^n}^{t^{n+1}} V\hat{\boldsymbol{u}}(L,t)\exp\left[\frac{\lambda}{R}(t-t^n)\right]\mathrm{d}t = \int_{t^n}^{t^{n+1}} V\left[U_N(t^n)\gamma_n(t) + U_N(t^{n+1})\gamma_{n+1}(t)\right]\exp\left[\frac{\lambda}{R}(t-t^n)\right]\mathrm{d}t, \tag{18}$$

where the interpolation functions γ_n and γ_{n+1} are appropriate piecewise-linear polynomials. This results in part of the integral adding to the coefficient for the unknown $U_N(t^{n+1})$, and the remainder involving known information and therefore contributing to the right side of the equation. While more elaborate schemes are discussed later in this paper, this simple approximation is reasonable in many cases.

Finally, the fifth integral involves the source or sink function in the equation. For a continuous function

$f(x,t)$, the integral may be evaluated numerically within the interior of the domain. Or, if the function is sufficiently simple, analytical evaluation may be used. The more complex case of point singularities is dealt with in the next section.

3. Extensions for practical problems

This section extends the framework of Section 2 in various ways. A wide range of extensions has been developed, and these are somewhat arbitrarily classified as spatial, temporal, and physical extensions. A given implementation can and has combined more than one of these concepts.

3.1. Basic spatial extensions

3.1.1. Multiple spatial dimensions, variable coefficients, conservative form

A rather general approach to these extensions was first formulated in [48], based in part on [5]. That formulation did not contain a reaction term, but we include one here to make this an extension of (8). For $R = R(\vec{x},t)$, $\vec{V} = \vec{V}(\vec{x},t)$, $\mathbf{D} = \mathbf{D}(\vec{x},t)$, $\lambda = \lambda(\vec{x},t)$, $f = f(\vec{x},t)$, the analogue of (1) is

$$(Ru)_t + \nabla\cdot(\vec{V}u - \mathbf{D}\nabla u) + \lambda u = f. \tag{19}$$

Multiply by the test function $w_i^{n+1}(\vec{x},t)$, where i is now a multi-dimensional index, note that $(Ru)_t w + \nabla\cdot(\vec{V}u - \mathbf{D}\nabla u)w = (Ruw)_t - Ruw_t + \nabla\cdot((\vec{V}u - \mathbf{D}\nabla u)w) - (u\vec{V}\cdot\nabla w - \mathbf{D}\nabla u\cdot\nabla w)$, and integrate over $\Omega_x\times\Omega_t$ (where Ω_x is now multi-dimensional) to obtain this extension of (8):

$$\begin{aligned}
&\int_{\Omega_x}\int_{\Omega_t}(Ruw_i^{n+1})_t\,\mathrm{d}t\,\mathrm{d}\vec{x} + \int_{\Omega_t}\int_{\Omega_x}\nabla\cdot((\vec{V}u - \mathbf{D}\nabla u)w_i^{n+1})\,\mathrm{d}\vec{x}\,\mathrm{d}t\\
&\quad + \int_{\Omega_t}\int_{\Omega_x}\mathbf{D}\nabla u\cdot\nabla w_i^{n+1}\,\mathrm{d}\vec{x}\,\mathrm{d}t\\
&\quad + \int_{\Omega_t}\int_{\Omega_x}u(-Rw_{it}^{n+1} - \vec{V}\cdot\nabla w_i^{n+1} + \lambda w_i^{n+1})\,\mathrm{d}\vec{x}\,\mathrm{d}t\\
&\quad = \int_{\Omega_t}\int_{\Omega_x} f w_i^{n+1}\,\mathrm{d}\vec{x}\,\mathrm{d}t.
\end{aligned} \tag{20}$$

Then the ensuing extension of (12), imposing the constraint

$$-R(\vec{x},t)w_t - \vec{V}(\vec{x},t)\cdot\nabla w + \lambda(\vec{x},t)w = 0, \tag{21}$$

is

$$\begin{aligned}
&\int_{\Omega_x}(Ruw_i^{n+1})(\vec{x},t^{n+1})\,\mathrm{d}\vec{x} - \int_{\Omega_x}(Ruw_i^{n+1})(\vec{x},t^{n})\,\mathrm{d}\vec{x}\\
&\quad + \int_{\Omega_t}\int_{\partial\Omega_x}(\vec{V}u - \mathbf{D}\nabla u)\cdot\vec{n}w_i^{n+1}\,\mathrm{d}S\,\mathrm{d}t\\
&\quad + \int_{\Omega_t}\int_{\Omega_x}\mathbf{D}\nabla u\cdot\nabla w_i^{n+1}\,\mathrm{d}\vec{x}\,\mathrm{d}t = \int_{\Omega_t}\int_{\Omega_x} f w_i^{n+1}\,\mathrm{d}\vec{x}\,\mathrm{d}t.
\end{aligned} \tag{22}$$

This is a direct approximation of the *conservative form* (19); most Eulerian–Lagrangian methods start from a nonconservative form instead. The test function will satisfy the adjoint Eq. (21), from which it can be determined as follows.

In 1-D, with variable coefficients, note that (5) is still appropriate, simply making $V = V(x,t)$, $R = R(x,t)$. In (6), the exponents must be replaced with integrals, viz.:

$$\begin{aligned}
&w_i^{n+1}(x^*(t),t) = \left(\frac{x - x_{i-1}}{\Delta x_{i-1}}\right)\exp\left(\int_{t^n}^{t}\frac{\lambda(x^*(\tau),\tau)}{R(x^*(\tau),\tau)}\,\mathrm{d}\tau\right),\\
&\quad x_{i-1}\leqslant x\leqslant x_i,\ \ t^n < t < t^{n+1},
\end{aligned} \tag{23}$$

etc., where $x^*(t)$ is the point at time t corresponding to x at time t^{n+1} along the characteristic curve, i.e., in an analogue of (7) we have

$$\begin{aligned}
&x^*(t) \equiv X(t;x,t^{n+1}) \equiv x - \int_{t}^{t^{n+1}}\frac{V(x^*(\tau),\tau)}{R(x^*(\tau),\tau)}\,\mathrm{d}\tau,\\
&\quad x_{i-1}\leqslant x\leqslant x_{i+1},\ \ t^n < t < t^{n+1}.
\end{aligned} \tag{24}$$

Thus, the linear factor in (23) is constant along characteristics. In practice, (23) and (24) must be approximated, meaning that the constraint (21) is satisfied approximately, rather than exactly as in (9). In multiple dimensions, the unmodified piecewise-linear functions can be used to form tensor-product test functions, e.g.,

$$\begin{aligned}
&w_{ij}^{n+1}(x^*(t),y^*(t),t)\\
&\quad = \left(\frac{x - x_{i-1}}{\Delta x_{i-1}}\right)\left(\frac{y_{j+1} - y}{\Delta y_j}\right)\exp\left(\int_{t^n}^{t}\frac{\lambda(x^*(\tau),y^*(\tau),\tau)}{R(x^*(\tau),y^*(\tau),\tau)}\,\mathrm{d}\tau\right),\\
&\quad x_{i-1}\leqslant x\leqslant x_i,\ y_j\leqslant y\leqslant y_{j+1},\ t^n < t < t^{n+1}.
\end{aligned} \tag{25}$$

The FV-ELLAM test functions from (14) can be treated analogously.

The approximations of (23) and (24) can be viewed as solving the associated ordinary differential equations analogous to (4) and (5) exactly with approximate values of λ/R and $\vec{V}/R$. It is convenient to suppose that R is exact, and that λ and $\vec{V}$ are approximated by $\overline{\lambda}(\vec{x},t)$ and $\overline{\vec{V}}(\vec{x},t)$, respectively. Then, in place of (21), we have

$$-Rw_t - \vec{V}\cdot\nabla w + \lambda w = -(\vec{V} - \overline{\vec{V}})\cdot\nabla w + (\lambda - \overline{\lambda})w, \tag{26}$$

where the right-hand side can be considered an error or a residual. One could then, instead of dropping the fourth term on the left-hand side of (20), treat this term by approximating the right-hand side of (26). This was first suggested in [48] and implemented in [19]. Note that for global mass conservation, where $w \equiv 1$, the $\vec{V} - \overline{\vec{V}}$ term vanishes, but the $\lambda - \overline{\lambda}$ term must be accounted for precisely in a spatially-integrated-average sense if mass-balance errors are to be avoided.

Particle-tracking algorithms: Tracking is important in determining the backtracked point x^* in (7) that defines an ELLAM test function, and also in numerical

integration of the second, third and fourth integrals in Section 2.3 (old-time-level spatial and inflow/outflow boundary integrals). This has been handled in many papers by various standard Euler or Runge–Kutta methods that we shall not describe here. Some calculations have used a "semi-analytical" approach formulated in [46], which is exact for flow (velocity) fields of the following form on Cartesian grids: on each space-time cell,

$$\begin{aligned}\vec{V}(x,y,z,t) &= (v^x(x,t), v^y(y,t), v^z(z,t)),\\ &= (a+bx+ct+dxt, e+fy+gt+hyt,\\ &\quad i+jz+kt+lzt),\end{aligned} \tag{27}$$

v^x is continuous in x and discontinuous in y and z across cell faces, and continuous in t across time steps; v^y and v^z are analogous. This is a lowest-order Raviart–Thomas (RT_0) velocity [42] in space at each time step, like the "linear" velocity of MODFLOW [32,37], with continuous linear interpolation in time. This builds on earlier semi-analytical work that assumed steady flow ($c = d = g = h = k = l = 0$ in (27)) [40] or a piecewise-constant time derivative ($d = h = l = 0$) [36].

Mixed finite element method for the flow field: In problems with heterogeneous permeability or formation properties, mixed finite element methods are known to yield more accurate flow fields. Also in view of tracking algorithms designed for the flow fields obtained from the RT_0 mixed method, as just discussed, it is natural to consider coupling an ELLAM transport code to a flow model based on RT_0, as done in [62]. In that reference, these methods were applied to 2-D incompressible miscible displacement (solute transport with concentration-dependent viscosity), including point sources and sinks. An analogous development for compressible flow was presented in [63] and will be extended to single-phase multicomponent flow in a forthcoming paper.

3.1.2. 3-D implementations

Practical issues motivated by 3-D applications were discussed in [9]. The general framework described in this section has been implemented in 3-D for both FE-ELLAM [7] and FV-ELLAM [7,27]. Some numerical results from these implementations will be presented in Section 5. The version of FV-ELLAM in [27] is publicly available as part of the USGS MOC3D codes (see [26,27,47] for details).

3.1.3. Sources and sinks

Interior sources and sinks, such as wells, present difficulties to Lagrangian-based methods because of diverging and converging flow fields. In particular, the velocity representation of (27) cannot be the basis of accurate tracking for a *strong source* (resp. *sink*), one in which the flux across all faces of the source cell is outward (resp. inward). For example, if the flow is radially symmetric from the cell center, the interpolation of (27) would yield a velocity of zero at the center, precisely the opposite of the expected increase in magnitude near the center.

A remedy for this problem was developed in [25], and the essential ideas will be described here. A strong source cell is treated as if there is instantaneous mixing throughout the cell, with influx at the specified source concentration c_{inj} and efflux at the resident concentration $U(t)$, which is spatially constant in the cell. It follows that the source-cell concentration over the time step $t^n \leqslant t \leqslant t^{n+1}$ is

$$U(t) = U(t^n) + (c_{inj} - U(t^n))(1 - \mathrm{e}^{-q(t-t^n)/v}), \tag{28}$$

where q is the source flow rate and v is the volume of the source cell. Because (28) determines $U(t)$ in the source cell, no discrete ELLAM equation is needed for that cell. The efflux from that cell contributes to the right-hand sides of the discrete equations for the cells that receive the efflux, via numerical integrals of the inflow-boundary type (see third integral in Section 2.3) with a fixed-concentration boundary condition and no diffusive flux (which is neglected in view of the distributed source). These integrals involve one time dimension (hence, sub-time steps) and 0, 1, or 2 space dimensions, with forward tracking of integration points. To conserve mass exactly, each point carries the average source concentration over its sub-time step (t_k, t_{k+1}), i.e.,

$$\overline{U}(t_k, t_{k+1}) = \frac{1}{t_{k+1} - t_k} \int_{t_k}^{t_{k+1}} U(t)\,\mathrm{d}t,$$

which is determined analytically from (28).

In a strong sink cell, the concentration is unknown, so that a discrete ELLAM equation is needed. Mass that tracks into this cell at any time during the time step is included on the right-hand side of this discrete equation, i.e., the mass cannot leave for another cell, and no tracking within the cell is necessary. The source term $f(x,t) = qU(t)/v$ is used. If greater temporal resolution of $U(t)$ is desired, concepts analogous to the discretized outflow boundary discussion in Section 3.2.2 can be applied. In a *weak source* (resp. *sink*), where the ambient flow is strong enough to create an inward (resp.outward) flux across at least one face of the cell, the usual discrete equation and the usual tracking based on (27) are kept.

3.1.4. Inactive cells

Many problems with irregular domains are discretized with inactive cells to approximate the shape of the domain. This is addressed in [27], where there is no test function associated with an inactive cell. In a cell adjacent to an inactive cell, if the inactive cell's test function would have been $w \neq 0$ had the cell been active, then w is distributed among the other nonzero test functions in proportion to their values; thus, the correct total weight is maintained.

3.1.5. Other work

The general formulation of [48] was implemented in [66] for 2-D advection–diffusion, with results for a rotating Gaussian hill. Early studies of variable coefficients in 1-D include [23] for advection–diffusion and [59] for advection–diffusion–reaction with biodegradation. A series of papers [3,52,56,57,64] considered coefficient interfaces in 1-D, with a technique of marching across the domain from the inflow to the outflow boundary, treating interface conditions as internal boundaries. Variable-coefficient 2-D formulations appeared for single-phase [24,55], reactive [60], and two-phase [6] flow. Sources and sinks were also considered in [2,26,27, 47,54,62,63].

3.2. Time-stepping procedures

The usual time-stepping procedure in ELLAM studies has been first-order backward Euler along characteristics. In (12), this applies to the diffusion and source terms. Considering the diffusion term, with the test function w_i^{n+1} as in (6) (Fig. 1), the nonzero contributions occur where $w_i^{n+1}(x,t) \neq 0$; call this space-time region Ω_i^{n+1}. Defining the characteristic direction τ such that

$$\frac{\partial w}{\partial \tau} \equiv \frac{\partial w}{\partial t} + \frac{V}{R}\frac{\partial w}{\partial x}, \tag{29}$$

we can parametrize Ω_i^{n+1} by

$$(X(\tau;x,t^{n+1}),\tau) \equiv \left(x - \frac{V}{R}(t^{n+1}-\tau),\tau\right),$$
$$x_{i-1} \leqslant x \leqslant x_{i+1}, \quad t^n < \tau < t^{n+1}. \tag{30}$$

Then the diffusion is approximated by backward Euler in time, viz.

$$D\int\int_{\Omega_i^{n+1}} \frac{\partial u}{\partial x}\frac{\partial w_i^{n+1}}{\partial x}\,\mathrm{d}x\,\mathrm{d}\tau \approx D\Delta t^n \int_{x_{i-1}}^{x_{i+1}} \frac{\partial u}{\partial x}(x,t^{n+1})\frac{\partial w_i^{n+1}}{\partial x}(x,t^{n+1})\,\mathrm{d}x. \tag{31}$$

This is the standard integral that would be obtained in a backward-Euler finite-element formulation. The source term is treated analogously. For interior test functions that are zero on inflow and outflow boundaries, the resulting discrete equations in the constant-coefficient setting of (12) are the same as those of the modified method of characteristics (MMOC) [17], which is an Eulerian–Lagrangian predecessor of ELLAM. For the FV-ELLAM test functions in (14), the same concepts apply, with appropriate treatment of the derivatives as before. For variable coefficients, the simple formula in (30) is replaced with (24), but because the backward-Euler approximation needs values at time t^{n+1} only, the form in (31) remains the same. This simplicity is the reason why backward Euler has been most often used. As with most Eulerian–Lagrangian methods, first-order time stepping in the characteristic direction, which follows the flow and experiences relatively small changes in the solution, is sufficiently accurate for many problems, even with large time steps (large Courant numbers).

3.2.1. Second-order Runge–Kutta

In [1], a more accurate second-order Runge–Kutta time-stepping scheme was developed for 1-D advection–diffusion with FE-ELLAM. This is more complicated, because it must use values at times earlier than t^{n+1} in integrals like (31), so that the approximations of (23) and (24) are critical. In particular, Heun's method was used to approximate (24), with $R \equiv 1$:

$$X(\tau;x,t) \approx Y(\tau;x,t) \equiv x - \frac{t-\tau}{2}[V(x,t) + V(x-(t-\tau)V(x,t),\tau)]. \tag{32}$$

Then the approximation (31) was replaced with a trapezoidal rule

$$D\int\int_{\Omega_i^{n+1}} \frac{\partial u}{\partial x}\frac{\partial w_i^{n+1}}{\partial x}\,\mathrm{d}x\,\mathrm{d}\tau \approx \frac{D\Delta t^n}{2}\left[\int_{x_{i-1}}^{x_{i+1}} \frac{\partial u}{\partial x}(x,t^{n+1})\frac{\partial w_i^{n+1}}{\partial x}(x,t^{n+1})\,\mathrm{d}x + \int_{x_{i-1}}^{x_{i+1}} \frac{\partial u}{\partial x}(x^*(t^n),t^n)\frac{\partial w_i^{n+1}}{\partial x}(x^*(t^n),t^n)\,\mathrm{d}x\right], \tag{33}$$

where $x^*(t^n) = Y(t^n;x,t^{n+1})$ from (32). Eq. (33) applies if w_i^{n+1} is zero on the inflow and outflow boundaries (i.e., an interior test function); otherwise, some additional terms are required [1]. The expected global order of the approximations is $O(\Delta x^2 + \Delta t^2)$. Versions based on both backward and forward tracking for the spatial integral at the old time level (second integral in Section 2.3) were developed. The second-order scheme was advantageous in cases with fine grids and large time steps, where the time-truncation error of backward Euler would be significant. Other papers have considered second-order Runge–Kutta time stepping for FV-ELLAM for 1-D advection–diffusion [2], and FE-ELLAM for advection–reaction in 1-D [54] and 2-D [60].

3.2.2. Discretization of outflow boundaries

This was considered in 1-D in the original ELLAM papers [11,45]. If the Courant number $Cr = V\Delta t^n/\Delta x$ is significantly larger than 1, it is natural to discretize the space-time outflow boundary in time, so as to describe the outflowing solution to the same resolution as the interior solution. The corresponding test functions (6) for a constant velocity field with $Cr \approx 2$ are depicted schematically in Fig. 3. For a test function such as w_{N+1}^{n+1} in Fig. 3, which is zero in the spatial domain at time t^{n+1},

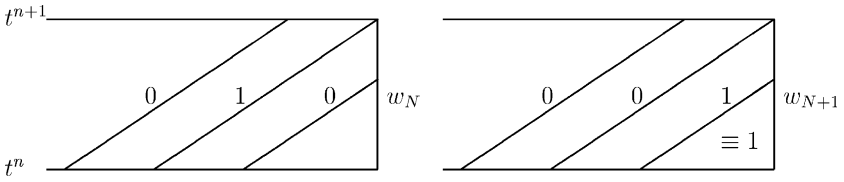

Fig. 3. Test functions near an outflow boundary.

and with a zero-diffusive-flux outflow boundary condition, (12) becomes

$$\int_{t^n}^{t^{n+1}} Vu(L,t)w_{N+1}^{n+1}(L,t)\,\mathrm{d}t + D\int\int_{\Omega_{N+1}^{n+1}} \frac{\partial u}{\partial x}\frac{\partial w_{N+1}^{n+1}}{\partial x}\,\mathrm{d}x\,\mathrm{d}\tau = \int_{\Omega_x} Ru(x,t^n)w_{N+1}^{n+1}(x,t^n)\,\mathrm{d}x + \int\int_{\Omega_{N+1}^{n+1}} fw_{N+1}^{n+1}\,\mathrm{d}x\,\mathrm{d}\tau. \tag{34}$$

The analogue of the backward-Euler approximation (31) replaces the D integral in (34) with an integral in t at $x = L$, which vanishes by the boundary condition. Here the unknown $u(L,t)$, $t^n < t \leqslant t^{n+1}$, involves additional trial-function degrees of freedom, matching the number of additional test functions. Note that (34) applies equally well to the indicated (parabolic) advection–diffusion–reaction problem and to the (hyperbolic) advection–reaction problem with $D = 0$; there is no change in the formulation from one case to the other, and in particular no artificial boundary conditions are needed. In either case, the known value $u(L,t^n)$ closes the system of equations. The usual incidence structure of the discrete matrix is preserved if the unknowns are numbered as suggested in Fig. 3.

In 2-D, the discretized outflow boundary involves the tangential space dimension as well as the time dimension, in a manner complementary to Fig. 2. The number of outflowing degrees of freedom at each spatial boundary point is essentially the Courant number in the normal direction. This has been implemented for advection–reaction equations in [60]. A similar effect has been obtained for advection–diffusion equations in [24] through the use of finer numerical integration in time at outflow boundaries. Either approach can be used to treat sinks as well. As in 1-D, the usual matrix structure is preserved, except for slight modifications at the corners of a structured spatial grid.

3.2.3. Local time stepping

The space-time finite-element formulation of ELLAM is a natural framework for local time stepping. This was combined with a discretized outflow boundary in [14] for the 1-D two-phase Buckley–Leverett equation, which can lead to outflow boundary layers. The space-time grids, without and with a boundary layer, are sketched for $Cr \approx 4$ in Fig. 4. For the second-order Runge–Kutta ELLAM, space-time local refinement was developed for 1-D linear advection–reaction equations in [53]. Physical and numerical interfaces in space and time were treated with a domain decomposition method designed for general space-time partitions. Grid refinement was based on a posteriori error estimators.

3.2.4. Operator splittings

The splitting in Eq. (4) is not the only one that could be considered. In the context of 1-D advection–diffusion–reaction with biodegradation, [59] considered a variety of possibilities. Other than (4), the principal alternative suggested by that work was (4) without the λw term, which then leaves an additional integral $\lambda\int\int uw_i^{n+1}\,\mathrm{d}x\,\mathrm{d}t$ on the left-hand side of (12). The test function is constant along characteristics in this case. Subsequent work has preferred the splitting in (4).

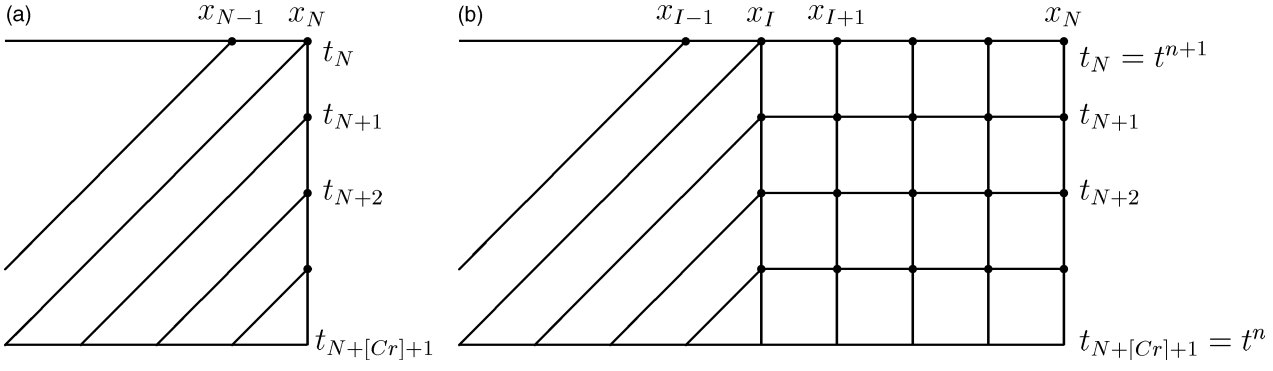

Fig. 4. (a) Outflow boundary elements. (b) Boundary-layer elements.

3.3. Physical extensions

This subsection considers generic physical extensions of the discretized equations, not specialized to particular applications. Applications are addressed in Section 5.

3.3.1. Compressibility

The extension of ELLAM concepts to compressible transport equations is straightforward. Assuming that the pressure $p(\vec{x},t)$ is known from a flow equation, and hence that the porosity $\phi(\vec{x},p)$ and the density $\rho=\rho(p)$ are determined, mass conservation is expressed by the following modification of (19):

$$(R\rho u)_t+\nabla\cdot(\vec{\sigma}u-\mathbf{D}(\vec{\sigma},p)\nabla u)+\lambda\rho u=\rho f, \tag{35}$$

where ϕ is absorbed into R, and $\vec{\sigma}(\vec{x},t)=\rho\vec{V}$ is the mass flux. The nonlinear couplings to the flow equation create higher-level complexities, but once a numerical decoupling is chosen, the application of ELLAM to (35) involves nothing beyond the techniques developed for (19). In particular, in coefficient quotients such as $\vec{V}/R$ and λ/R, the new factors of ρ cancel. In combination with a mixed method for flow, this was implemented in [63]. A single-phase multicomponent extension is being developed in a forthcoming paper.

3.3.2. Nonlinear flux

Unsaturated flow can be formulated in such a way that the nonlinearities are confined to the flow equation, and the transport equation is qualitatively similar to (19) [6]. The 1-D two-phase Buckley–Leverett problem yields a nonlinear transport equation and has been solved with ELLAM in [14,57]. The analogue of Vu in (24) is a nonlinear flux $V(u)$ that can be normalized to an increasing function with $V(0)=0$, $V(1)=1$. The essential idea, based on [18], was to split the nonlinear flux into two terms,

$$V(u)=\overline{V}(u)+b(u)u, \tag{36}$$

where $\overline{V}(u)$ would yield the correct physical (possibly shock) solution $\overline{u}$ of the hyperbolic conservation law $\overline{u}_t+(\overline{V}(\overline{u}))_x=0$ with the old-time-level solution $u(t^n)$ as initial data. In some cases, $\overline{V}(u)$ is the convex hull of the function $V(u)$; in general, an approximation of $\overline{V}(u)$ could be used. The choice of $\overline{V}(u)$ is such that $\overline{u}$ does not develop shocks. This enables $\overline{u}$ to be substituted for u in the nonlinear flux to obtain a linear operator, which has an adjoint, so that ELLAM can be applied. The residual b term remains in the analogue of (22), grouped with diffusion (capillary forces), and tends to cancel it.

3.3.3. Compositional model

The preceding approach appears to be specialized to relatively simple two-phase flow systems that can be modeled with a nonlinear flux function. For more complex systems, such as three-phase black-oil and compositional models from the petroleum industry, a more general formulation will be needed. A first attempt was implemented in [41] for compositional reservoir simulation. This procedure solves a flow equation to obtain a pressure and a total velocity $\vec{V}$. Associated with each hydrocarbon component i is a component velocity $\vec{V}^i$ of the form

$$\vec{V}^i=\left(\frac{N_{\mathrm{o}}^i}{N^i}\frac{f_{\mathrm{o}}}{S_{\mathrm{o}}}+\frac{N_{\mathrm{g}}^i}{N^i}\frac{f_{\mathrm{g}}}{S_{\mathrm{g}}}\right)\vec{V}, \tag{37}$$

where N^i is the total number of moles of component i in all phases, N_{o}^i (resp. N_{g}^i) is the number of these moles in the oil (resp. gas) phase, $f_{\mathrm{o}}=\lambda_{\mathrm{o}}/(\lambda_{\mathrm{o}}+\lambda_{\mathrm{g}})$ is the fractional mobility of oil, S_{o} is oil saturation, and f_{g} and S_{g} are analogous for the gas phase. Thus, the vectors $\vec{V}^i$ and $\vec{V}$ have the same direction. ELLAM uses the velocity $\vec{V}^i$ in the conservation equation for component i. Other capillary and gravity terms that deviate from the total-velocity direction are separately treated explicitly. This could impose stability constraints that could negate some of the advantages of ELLAM (e.g., lack of Courant-number restrictions); for a robust implementation, full interstitial phase velocities including implicit capillarity and gravity might be required. Such a formulation might be based on tracking of mixtures within each phase, according to the full phase velocities, followed by flash calculations based on the total of all fluids arriving in a cell through all phases.

4. Error analysis

Theoretical analysis of ELLAM has been spearheaded by Wang, with the assistance of Ewing and others [20,21,50,51,58,61,67]. To date, error estimates have been proved only for FE-ELLAM applied to single scalar linear equations. However, within that limitation, the results are strong and significant. Problems in 1-D and 2-D, from pure advection to advection–diffusion–reaction (thus, any Péclet number from 0 to ∞), with constant or variable coefficients, and with all types of boundary conditions have been considered. Large (greater than 1) and small (less than 1) Courant numbers have been analyzed. With piecewise-linear trial functions and backward-Euler time stepping, optimal-order L^2 convergence of $\mathrm{O}(\Delta x^2+\Delta t)$ has been proved in all cases. A literature survey of theoretical work on other methods can be found in [50]; it can be summarized with the statement that, to our knowledge, comparable optimal-order estimates are not known for any other method over the same range of parameter values.

The most comprehensive early analysis appeared in [61], covering 1-D advection–diffusion with constant coefficients and all combinations of inflow and outflow boundary conditions (Dirichlet, Neumann, total flux). The basic error estimate has the form

$$\max_n \|U(\cdot,t^n)-u(\cdot,t^n)\|_{L^2(x)} + \|U(L,\cdot)-u(L,\cdot)\|_{L^2(t)} \leqslant C(\Delta x^2+\Delta t), \quad (38)$$

where U is the ELLAM approximation, u is the exact solution, and C is a constant independent of Δx and Δt. The second term in (38) estimates the error of the approximation to the outflowing concentration; if the outflow boundary condition is Dirichlet, in which case the outflowing concentration is known, this is replaced with an estimate of $\|\partial U/\partial x(L,\cdot)-\partial u/\partial x(L,\cdot)\|$ that is essentially $O(\Delta t/\sqrt{\Delta x})$. A result analogous to this was obtained in all of the papers, assuming sufficient smoothness of the exact solution u (typically H^2, two square-integrable derivatives). If u is especially smooth (H^3) and the grid is uniform, a "superconvergence" result (higher order of convergence at certain points than is possible globally) also holds for the solution gradient (diffusive flux) at cell faces:

$$\left\{\sum_n\left(\sum_{i=1}^N\left|\frac{\partial U}{\partial x}(x_{i-1/2},t^n)-U(x_{i-1/2},t^n)\right|^2\Delta x\right)\Delta t\right\}^{1/2} \leqslant C(\Delta x^2+\Delta t). \quad (39)$$

In the sum in (39), Δt is modified near the inflow boundary to be the time in which influx travels from the boundary to $x_{i-1/2}$, if that time is less than Δt. This type of result was obtained in the papers that included diffusion.

The arguments to obtain these estimates are more complex than those for MMOC [17] and related methods. The just-mentioned modification of Δt introduces a degeneracy into the diffusion near an inflow boundary, and the discretization of the outflow boundary in certain cases can cause further indefiniteness in the equations. Techniques to overcome these theoretical difficulties were begun in [61].

Reactions were first analyzed in [20], which treated 1-D advection–reaction equations with constant coefficients. The test functions satisfied (4) and hence had the form of (6). Without diffusion, the only boundary condition is an inflow Dirichlet condition. The estimate (38) was shown, requiring additional smoothness (H^3) on u. Then the scope of [61] and [20] was combined in [58], with advection–diffusion–reaction. The estimates (38) and (39) were as in [61], with an additional technique that removed a $\Delta x^2\|\partial u/\partial t\|_{L^2(H^2)}$ term from the results of [61], where $L^2(H^2)$ refers to a norm that involves L^2 in time and H^2 in space. This introduced a new term $\Delta x^2\|u\|_{L^\infty(H^3)}$ in cases of small Courant number. The idea was that in advection-dominated problems, a τ-derivative (following the flow, with τ defined as in (29)) would be smaller than a t-derivative, making it desirable to remove $\|\partial u/\partial t\|$. Since the truncation error of backward Euler involves second time derivatives $\partial^2 u/\partial t^2$, which had already been replaced by $\partial^2 u/\partial\tau^2$ in the analysis of [61], it is difficult to tell whether the removal of the lower time derivative $\Delta x^2\|\partial u/\partial t\|_{L^2(H^2)}$ at the cost of $\Delta x^2\|u\|_{L^\infty(H^3)}$ is valuable.

Variable-coefficient 1-D advection–reaction [21] and advection–diffusion–reaction (all combinations of boundary conditions) [50] were then analyzed. In [21], (38) of the form proved in [58] was obtained for two ELLAM schemes; in one of these, errors in tracking through variable velocity fields were compensated for by introducing residual advective terms into the scheme, along the lines of the $V-\overline{V}$ term in (26). Without diffusion, the H^3-dependence was already necessary as in [20], so that the removal of $\Delta x^2\|\partial u/\partial t\|_{L^2(H^2)}$ as in [58] was cost-free in this case. In [50], (38) and (39) were shown for two analogous schemes, with a nonuniform (but quasi-uniform) grid. The $\Delta x^2\|\partial u/\partial t\|_{L^2(H^2)}$ term could not be removed in this case, or in the 2-D cases discussed next.

Finally, 2-D variable-coefficient advection–diffusion (total-flux inflow and Dirichlet outflow boundary conditions) [51] and advection–reaction [67] equations were analyzed. For advection–diffusion, (38) and (39) were shown, with (38) requiring $W^{2,\infty}$-smoothness (two bounded derivatives). The multi-dimensionality led to this additional smoothness requirement. For advection–reaction, (38) was obtained, with H^3-smoothness needed as in [20,21]; all of the zero-diffusion results have required this.

One limitation of this range of results is that they all depend on at least H^2-smoothness of the solution, an assumption that can be violated as the Péclet number tends to ∞. That is, the results apply to advection of smooth solutions, but not to shocks. Another limitation is that the results assume exact integration, and as is well-known for characteristic Galerkin methods, numerical integration for hyperbolic equations (infinite Péclet number) can lead to stability problems [38].

5. Applications

ELLAM approximations have been applied to a number of test cases and practical problems involving contaminant transport in porous media. These include linear advection–diffusion equations in one, two, and three dimensions; linear and nonlinear advection–diffusion–reaction equations in one and two dimensions; simulations involving contaminant transport in both saturated and unsaturated zones of the subsurface; and nonlinear transport associated with two-phase flow problems.

Standard one-dimensional problems have been reported by many authors, beginning with the original publications of Celia et al. [11] and Russell [45] and going through recent publications of Binning and Celia [7] and Heberton et al. [27]. While these and others demonstrate the effectiveness of the algorithm, two publications stand out in terms of comprehensive

comparisons of ELLAM approximations to other numerical approaches. Wang et al. [54] and Al-Lawatia et al. [1] have compared ELLAM to a number of other approaches, using the standard one-dimensional test problems involving a Gaussian hill and a square wave, each transported along a one-dimensional domain. In those papers, ELLAM using Runge–Kutta methods to track along characteristics were compared against Galerkin, quadratic Petrov–Galerkin (QPG), cubic Petrov–Galerkin (CPG), continuous and discontinuous Galerkin methods (CGM, DGM), streamline diffusion finite element methods (SDM), monotonic upstream-centered scheme for conservation laws (MUSCL), and essentially nonoscillatory methods (ENM). Versions of both forward tracking and back-tracking were used in the ELLAM approximations. Wang et al. [54] solved the case of zero diffusion, while Al-Lawatia et al. [1] solved cases with nonzero diffusion. Wang et al. [54] also included a numerical demonstration of convergence rates. In both of these papers, a range of time and space steps was used to solve the example problems, and error measures were used to demonstrate that the ELLAM solutions were consistently as good as or better than all other methods tested, while providing strong computational advantages because of the large allowable time steps. These comparisons were extended to two dimensions in [55,60], using the rotating cone problem as the test case. The range of numerical methods tested corresponded to those in the one-dimensional tests. Similar results were found.

Additional two-dimensional test problems have been presented by various authors [6,24,27]. In [27], a model two-dimensional radial flow and transport problem is solved, and the transport problem based on solute leaching into a nonuniform flow field first described and solved by Burnett and Frind [8]. Heberton et al. [27] also solved a series of transport problems in uniform flow fields, with flow direction varying with respect to grid direction, to test grid orientation effects. While observable, grid orientation effects were not significant.

Several three-dimensional problems have also been solved using the ELLAM algorithm. Heberton et al. [27] solved the transport equation in a uniform flow field, with a continuous point source. They also solved the three-dimensional version of the problem of Burnett and Frind [8] on a $141 \times 15 \times 91$ grid. Fig. 5 compares concentration contours obtained with (a) a modification of the 3-D finite-element model of Burnett and Frind (approximately 4,000 time steps) and (b) the MOC3D ELLAM model (7 time steps, Courant number $\approx$30). It is clear that ELLAM can obtain similar results with much larger time steps in this case. Binning and Celia [7] solved a similar problem, but with a patch boundary source along the inflow boundary. Binning and Celia [7] also solved a three-dimensional advection–diffusion transport problem using a spatially variable velocity

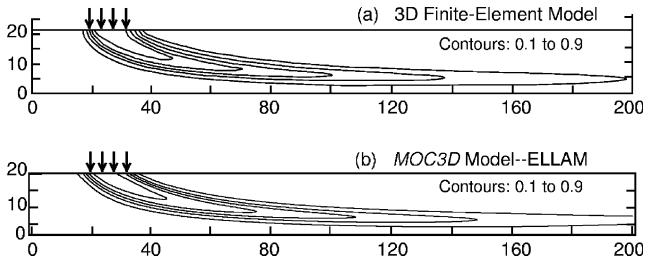

Fig. 5. Three-dimensional simulation results for nonuniform-flow test case in which $\alpha_{TH} = 10\alpha_{TV}$: (a) finite-element model (modified from [8, Fig. 8c]), (b) numerical ELLAM solution using $Cr = 30$. Source is indicated by arrows at the top of the vertical slice; contour interval is 0.2 relative concentration.

field and a three-dimensional patch source as part of the initial conditions. This case was modeled after the large-scale tracer experiments performed at the Cape Cod field site (see, for example, [33] for a description of the site). Binning and Celia [7] generated a spatially variable realization of the hydraulic conductivity field, based on measurements reported in [30], to generate a variable velocity field based on cell-centered finite differences. Tracking procedures using the method of Pollock [40] were used in a forward-tracking ELLAM algorithm, with piecewise linear trial functions, to model the transport of the nonreactive tracer bromide. Behavior of zeroth, first, and second moments of the concentration field follow the behavior demonstrated by the experimental plume [22], and the plume has the kind of irregular shape expected in this kind of transport system. A typical snapshot of the plume is shown in Fig. 6.

Nonlinear equations have also been solved using ELLAM. The three major problems that have been solved are (1) contaminant transport and biodegradation in saturated porous media, where the nonlinearity is associated with the reaction terms; (2) contaminant transport in unsaturated soils, where transport is coupled to a nonlinear flow equation (Richards' equation) and the transport is governed by nonlinear coefficients arising from the flow solution; and (3) two-phase flow equations where manipulation of the governing equations into Buckley–Leverett types of equations leads to nonlinear advective and diffusive fluxes that need to be handled in the context of ELLAM. Biodegradation was first modeled using ELLAM by Wang et al. [59]. A linearized version of the governing equations was solved using the general procedure outlined in [12]. For the case of aerobic biodegradation, the model two-equation system consisted of an equation for the contaminant and an equation for the concentration of oxygen. These equations are coupled through the reaction terms, which are nonlinear in the concentrations. The equations were solved sequentially, and comparison to example calculations reported earlier in [10,31] demonstrated the effectiveness of the ELLAM approach. A similar approach was followed by Våg et al. [49], who compared

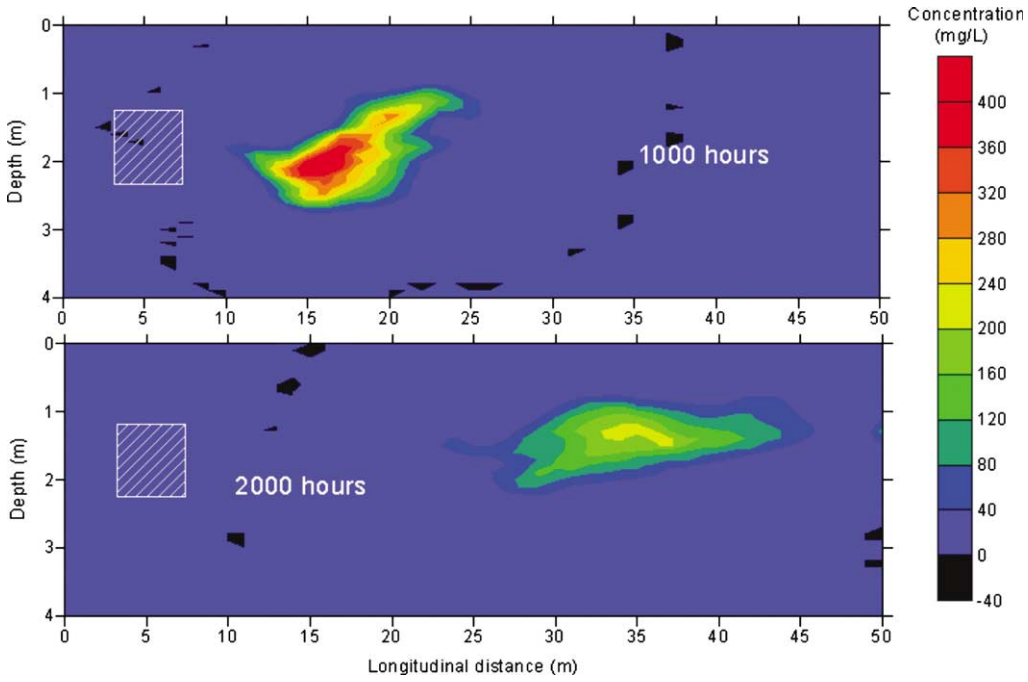

Fig. 6. Two snapshots of 3-D ELLAM solution for Cape Cod plume [7].

different linearization approaches, and described applications to problems in both groundwater hydrology (biodegradation of contaminants) and oil reservoirs (souring by sulfate reducing bacteria).

Models involving unsaturated flow and contaminant transport were developed in [6] and applied to flow and transport in both homogeneous and heterogeneous unsaturated soils in two spatial dimensions. Both conservative and nonconservative forms of the governing transport equation were used. Because of the complex multi-dimensional flow fields, the choice of equation forms was shown to depend in part on local versus global conservation properties inherent in the numerical representation of the flow field. The main application of the algorithm was to a field experiment carried out in the unsaturated zone at the Cape Cod field site (see [44] for a description of the experiments and the site). Heterogeneous soil properties were used to define the system, and the nonlinear flow and transport equations were solved. The ELLAM approximations captured spatial variability of the contaminant, and allowed for very efficient solutions for the transport problem.

While the transport solutions reported by Binning and Celia [6] for the unsaturated-zone problem were highly efficient, the flow part of the problem was solved by standard Eulerian methods and therefore required significant computational effort. To apply ELLAM types of approximations to two-phase flow problems, the general approach followed by Espedal and Ewing [18] can be followed. Dahle et al. [14] took this approach and solved Buckley–Leverett types of equations using an ELLAM approximation. The governing equation involves nonlinear advection and diffusion terms, with tendencies to form shock fronts. Because of the nonlinearities, characteristic tracking and equation solution must be performed iteratively. Dahle et al. [14] used ELLAM in combination with local time stepping procedures (to handle boundary layers) to solve the two-phase flow equation. Different combinations of boundary conditions were solved for a one-dimensional water-flood problem, which exhibits a very sharp front combined with a rarefaction wave. Solutions were shown to be excellent, including proper mass balances. Some of the mathematical details are described in Section 3.3.2.

A recent application of ELLAM approximations was reported [62,63] for miscible transport associated with injection/extraction well systems arranged in a five-spot pattern. In those simulations, compressible flow equations were solved using mixed finite element methods, providing accurate velocities for the ELLAM transport simulations. Examples included a range of mobility ratios, material heterogeneity, and tensor dispersions with different values of dispersivities and diffusion coefficients. Results demonstrated that the ELLAM allows large time steps while maintaining accurate solutions.

6. The ELLAM framework as a context for other related methods

6.1. Finite difference Eulerian–Lagrangian methods

Finite difference-based Eulerian–Lagrangian methods (ELM's) have been used in a variety of fields, including

ground-water transport [13] and surface-water transport [4]. This class of approximations again treats the advective transport in a characteristic framework, while treating the diffusive transport in an Eulerian framework. Because there is no weak form associated with these equations, the governing equation is typically written in nonconservative form. For typical flow and transport systems, this involves combination of the mass balance equation for the overall fluid phase with the mass balance for the individual component of the phase. One-point (in space) finite-difference approximations are written for the characteristic solutions, and this advective projection is then combined with the diffusive terms to yield an approximation at the new time level. The characteristic solution would typically follow a backtracking strategy, involving spatial location x_i at time t^{n+1} (see Fig. 1). The characteristic passing through that point is tracked back to time level t^n, and the associated spatial point, x_i^*, referred to as the 'foot of the characteristic', is located. In the simplest case, the resulting equation is

$$\widehat{U}_i^{n+1} = U(x^*, t^n), \tag{40}$$

where $\widehat{U}_i^{n+1}$ refers to the advective approximation for the unknown concentration at the new time level. Because x^* generally does not correspond to a nodal location, the value of the function at this location must be interpolated from nodal values. This interpolation is a critical step, and much effort has been spent to try to optimize the interpolation.

In the ELLAM context, we may view the FDELMs as approximations to the general ELLAM equation, where spatial integrals at time t^{n+1} are evaluated using one-point numerical integration, where that point is chosen as the nodal location x_i. This produces a lumped mass matrix. At the previous time level, t^n, again a one-point integration is used, with the integration point located at x^*. To compensate for the relatively poor approximation to the integral, higher order interpolants are often introduced to improve the evaluation at t^n. Boundary conditions are usually restricted to simple fixed-concentration or zero-diffusive flux conditions. The diffusive terms are typically treated with an implicit approximation, with standard finite difference approximations in space. Mass is typically not conserved. Overall, in the ELLAM context, FDELMs may be viewed as simplified approximations that use low-order interpolation at t^{n+1}, high-order interpolation at t^n, one-point approximations to the spatial integrals, and a simplified treatment of boundary conditions.

6.2. Characterisic Galerkin methods and the modified method of characteristics

Characteristic Galerkin methods form a broad class of finite element-based approximations in which advective fluxes are treated in a characteristic framework, while other terms are treated in an Eulerian type of framework. This method is usually attributed to Pironneau [39], with subsequent significant publications including [15,16,34,35]. While sometimes different in minor details, the Characteristic Galerkin Method overlaps broadly with the so-called MMOC [17]. The properties are similar to the FDELMs of the preceding subsection, except in the spatial integrals at times t^{n+1} and t^n. As is typical with Galerkin-type methods, the mass matrix is unlumped. This makes it easier for these methods to avoid numerical dispersion than it is for FDELMs, because the unlumped mass matrix can counteract the diffusive effects of interpolation at x^*. Thus, the high-order interpolation often used with FDELMs is typically not necessary, and is replaced with relatively low-order numerical integration. As with FDELMs, mass is generally not conserved, and general boundary conditions are difficult to treat.

6.3. Particle tracking methods

Particle tracking methods usually involve representation of dissolved mass as a cluster of discrete particles, each having a prescribed mass such that the total mass is preserved. Each of these particles is transported by forward tracking along characteristics. At prescribed time intervals, random motions are added to the particles to account for diffusion. If reactions are taking place, additional modifications need to be included, depending on the complexity of the reactions. Ideally, each particle maintains its own identity throughout the transport process, such that the main piece of information is the location and mass of the particle at any given time. A switch to concentration measures leads to mixing and loss of individuality for particles, and efforts are often made to avoid use of both particles and concentrations.

In the ELLAM context, forward tracking of integration points (see Eq. (24), tracked forward instead of backward) may be seen as analogous to particle tracking. In this case, each integration point carries with it an amount of mass, and it is transported along characteristics. However, because ELLAM is concentration-based, the masses transported by each integration point are "mixed" at the end of each time step, and the integration point locations are set back to their original locations for the next time step. Because packets of mass (particles) are not tracked continuously in ELLAM, but only between time steps, ELLAM cannot, in general, reproduce the particle tracking algorithm. However, for more complex problems such as those involving reactions, where the reactions are a function of local concentrations, particle methods must revert to concentrations to accommodate reaction terms. For such cases, particle methods approach the forward-tracking

ELLAM algorithm. Diffusion and dispersion terms are usually approximated by a random-walk algorithm in particle methods, such that an additional random displacement is applied at the end of the advective tracking step. In ELLAM algorithms, diffusion and dispersion terms are treated naturally in the context of the approximating equations.

6.4. USGS MOC algorithm

Finally, we compare the ELLAM approach to one of the most popular methods for solution of contaminant transport equations, the MOC method of the USGS [32]. In that method, discrete packets (finite volumes) of fluid are tracked via characteristic tracking over a time step. This procedure is analogous to the tracking of integration points in ELLAM. The USGS-MOC algorithm then converts the tracked mass into nodal concentrations, for the purpose of calculating changes in contaminant mass for each fluid volume due to diffusion and dispersion. These changes in mass are then applied to the solute mass in each of the individual packets of fluid, but the location of those packets is maintained. Therefore, while treating diffusion on a concentration basis, the random-walk part of the particle method is avoided. However, by keeping track of the location of the individual fluid packets, complete mixing within each cell at the end of each time step is avoided. This method suffers from a lack of mass conservation, although it often provides good numerical performance.

7. Conclusions and future work

ELLAM has been applied successfully to a wide variety of linear and nonlinear transport problems in one, two, and three dimensions. For some typical test problems, it has been shown to outperform other well-known methods, conserving mass while taking large, accurate time steps. For sufficiently smooth exact solutions, the theoretical results to date show optimal-order convergence over the full range of Péclet and Courant numbers.

A significant limitation in current ELLAM implementations is the absence of a mechanism to control nonphysical oscillations. ELLAM solutions will be oscillation-free on coarser grids than solutions from standard methods such as centered finite differences, but ELLAM will still oscillate on grids that are too coarse to assure three or four degrees of freedom across a front. It should be possible to combine the ELLAM formulation with a form of flux limiting, as has already been done for the modified method of characteristics [43]. This would minimize oscillations and would remove one of the principal obstacles to wider use of existing ELLAM codes.

The efficiency of existing implementations could be substantially improved. The backtracking and forward tracking that defines the space-time test and trial functions, and that contributes to numerical integration, can be done in parallel, because each tracked point is independent of all of the others. To date, this has not been implemented on parallel architectures. The tracking is a major part of the overall computational effort, especially when time steps are large and a point is tracked across several cells in a time step. Another issue of efficiency is the calculation of the mass integral at the old time level t^n. Existing algorithms are rather crude, either in accuracy or in the use of a large number of integration points, and large improvements should be possible.

The flexible framework of ELLAM lends itself naturally to more general space-time grids than have been investigated up to now. There is no conceptual barrier to the use of distorted or unstructured spatial grids. The formulation also accommodates space-time local refinement, with interface terms in the form of physically meaningful integrals. The efforts in this direction to date have been limited to one space dimension. Another natural use of ELLAM would be to extend the range of effectiveness of state-of-the-art "elliptic" methods, such as multigrid, which are most effective for self-adjoint (nonadvective) problems; ELLAM can handle all or most of the nonself-adjoint advection in many problems, leaving a self-adjoint or nearly self-adjoint problem that could be solved efficiently with elliptic methods. An analogous theme, improving the effectiveness of wavelets and multiresolution analysis for multidimensional advection–reaction problems, was pursued in [65], where an unconditionally stable explicit ELLAM scheme was developed.

The development of Eulerian–Lagrangian methods for complex fluid systems, such as three-phase black-oil and compositional models, is still in its infancy, particularly in three dimensions. Efforts in this direction will be ongoing, perhaps along the lines discussed in Section 3.3.3, with appropriate extensions of the source/sink treatment in Section 3.1.3. Finally, while there are many theoretical results for FE-ELLAM, there are presently none for its finite-volume counterpart. As the local conservation of the FV formulation and its compatibility with existing finite-difference codes make it attractive for applications, a firm theoretical foundation would be worthwhile.

Acknowledgements

The authors express their gratitude to colleagues Philip Binning, Helge Dahle, Richard Ewing, Rick Healy, Ismael Herrera, and Hong Wang, whose long-term contributions have been vital to the research documented here. The first author was supported in part by

NSF Grant No. DMS-0084438 and ARO Grant No. DAAG55-97-1-0171.

References

[1] Al-Lawatia M, Sharpley RC, Wang H. Second-order characteristic methods for advection–diffusion equations and comparison to other schemes. Adv Water Resour 1999;22:741–68.

[2] Al-Lawatia M, Sharpley RC, Wang H. A finite-volume Runge–Kutta ELLAM method for the solution of advection diffusion equations. SQU J Sci Technol 2001;6:67–83.

[3] Al-Lawatia M, Wang H. A nonoverlapping characteristic domain decomposition method for unsteady state advection–diffusion equations. In: Lai et al., editors. Eleventh International Conference on Domain Decomposition Methods. Bergen, Norway: Domain Decomposition Press; 1999. p. 151–8.

[4] Baptista AM. Solution of Advection-Dominated Transport by Eulerian–Lagrangian Methods Using Backward Methods of Characteristics, Ph.D. Dissertation, Department of Civil Engineering, MIT, 1987.

[5] Benqué JP, Ronat J. Quelques difficultés des modèles numériques en hydraulique. In: Glowinski VR, Lions JL, editors. Computing methods in applied sciences and engineering. Amsterdam: North-Holland; 1982. p. 471–94.

[6] Binning P, Celia MA. A finite volume Eulerian–Lagrangian localized adjoint method for solution of the contaminant transport equations in two-dimensional multiphase flow systems. Water Resour Res 1996;32:103–14.

[7] Binning P, Celia MA. A forward particle tracking Eulerian–Lagrangian localized adjoint method for solution of the contaminant transport equation in three dimensions. Adv Water Res 2002;25:147–57.

[8] Burnett RD, Frind EO. Simulation of contaminant transport in three dimensions, 2. Dimensionality effects. Water Resour Res 1987;23:695–705.

[9] Celia MA. Eulerian–Lagrangian localized adjoint methods for contaminant transport simulations. In: Peters A et al., editors. Computational Methods in Water Resources X, vol. 2. Dordrecht, Netherlands: Kluwer Academic Publishers; 1994. p. 207–16.

[10] Celia MA, Kindred JS, Herrera I. Contaminant transport and biodegradation, 1. A numerical model for reactive transport in porous media. Water Resour Res 1989;25:1141–8.

[11] Celia MA, Russell TF, Herrera I, Ewing RE. An Eulerian–Lagrangian localized adjoint method for the advection–diffusion equation. Adv Water Resour 1990;13:187–206.

[12] Celia MA, Zisman S. An Eulerian–Lagrangian localized adjoint method for reactive transport in groundwater, computational methods in subsurface hydrology. In: Gambolati G, et al., editors. Proceedings of 8th International Conference on Computational Methods in Water Resources. Southampton, UK: Computational Mechanics Publications; 1990. p. 383–92.

[13] Cheng RT, Casulli V, Milford S. Eulerian–Lagrangian solution of the convection–diffusion equation in natural coordinates. Water Resour Res 1984;20:944–52.

[14] Dahle HK, Ewing RE, Russell TF. Eulerian–Lagrangian localized adjoint methods for a nonlinear advection–diffusion equation. Comp Meth Appl Mech Engrg 1995;122:223–50.

[15] Dawson CN, van Duijn CJ, Wheeler MF. Characteristic-Galerkin methods for contaminant transport with nonequilibrium adsorption kinetics. SIAM J Numer Anal 1994;31:982–99.

[16] Dawson CN, Martinez-Canales ML. A characteristic-Galerkin approximation to a system of shallow water equations. Numer Math 2000;86:239–56.

[17] Douglas Jr J, Russell TF. Numerical methods for convection-dominated diffusion problems based on combining the method of characteristics with finite element or finite difference procedures. SIAM J Numer Anal 1982;19:871–85.

[18] Espedal MS, Ewing RE. Characteristic Petrov–Galerkin subdomain methods for two-phase immiscible flow. Comp Meth Appl Mech Engng 1987;64:113–35.

[19] Ewing RE, Wang H. An Eulerian–Lagrangian localized adjoint method with exponential-along-characteristic test functions for variable-coefficient advective–diffusive–reactive equations. In: Choi et al., editors. Proceedings of KAIST Mathematical Workshop, Analysis and Geometry, vol. 8, Taejon, Korea, 1993. p. 77–91.

[20] Ewing RE, Wang H. Eulerian–Lagrangian localized adjoint methods for linear advection or advection–reaction equations and their convergence analysis. Comput Mech 1993;12:97–121.

[21] Ewing RE, Wang H. An optimal-order estimate for Eulerian–Lagrangian localized adjoint methods for variable-coefficient advection–reaction problems. SIAM J Numer Anal 1996;33:318–48.

[22] Garabedian SP, LeBlanc DR, Gelhar LW, Celia MA. Large-scale natural gradient tracer test in sand and gravel, Cape Cod, Massachusetts: 2. Analysis of spatial moments for a non-reactive tracer. Water Resour Res 1991;27:911–24.

[23] Healy RW, Russell TF. A finite-volume Eulerian–Lagrangian localized adjoint method for solution of the advection–dispersion equation. Water Resour Res 1993;29:2399–413.

[24] Healy RW, Russell TF. Solution of the advection–dispersion equation in two dimensions by a finite-volume Eulerian–Lagrangian localized adjoint method. Adv Water Resour 1998;21:11–26.

[25] Healy RW, Russell TF. Treatment of internal sources in the finite-volume ELLAM. In: Bentley L, et al., editors. Computational Methods in Water Resources, vol. 2. Rotterdam: A.A. Balkema; 2000. p. 619–22.

[26] Heberton CI, Russell TF, Konikow LF, Hornberger GZ. Three-dimensional finite-volume ELLAM implementation. In: Bentley L, et al., editors. Computational Methods in Water Resources, vol. 2. Rotterdam: A.A. Balkema; 2000. p. 603–10.

[27] Heberton CI, Russell TF, Konikow LF, Hornberger GZ. A three-dimensional finite-volume Eulerian–Lagrangian localized adjoint method (ELLAM) for solute-transport modeling. Water-Resources Investigations Report 00-4087, US Geological Survey, Reston, VA, 2000. Ground Water, special issue on MODFLOW 2001 and Other Modeling Odysseys, in press.

[28] Herrera I. Localized adjoint methods: a new discretization methodology. In: Fitzgibbon WE, Wheeler MF, editors. Computational methods in geosciences. Philadelphia: SIAM; 1992. p. 66–77 [Chapter 6].

[29] Herrera I, Ewing RE, Celia MA, Russell TF. Eulerian–Lagrangian localized adjoint methods: the theoretical framework. Numer Meth PDE 1993;9:431–57.

[30] Hess KM, Wolf SH, Celia MA. Large-scale natural gradient tracer test in sand and gravel, Cape Cod, Massachusetts: 3. Hydraulic conductivity variability and calculated macrodispersivities. Water Resour Res 1992;28:2011–27.

[31] Kindred JS, Celia MA. Contaminant transport and biodegradation, 2. Conceptual model and test simulations. Water Resour Res 1989;25:1149–59.

[32] Konikow LF, Goode DJ, Hornberger GZ. A three-dimensional method-of-characteristics solute-transport model (MOC3D). US Geological Survey Water-Resources Investigations Report 96-4267, Reston, VA, 1996.

[33] LeBlanc DR, Garabedian SP, Hess KM, Gelhar LW. Large-scale natural gradient tracer test in sand and gravel, Cape Cod, Massachusetts: 1. Experimental design and observed tracer movement. Water Resour Res 1991;27:895–910.

[34] Li X, Wu W, Zienkiewicz OC. Implicit characteristic Galerkin method for convection–diffusion equations. Int J Numer Meth Engrg 2000;47:1689–708.

[35] Li X, Wu W, Cescotto S. Contaminant transport with non-equilibrium processes in unsaturated soils and implicit characteristic Galerkin scheme. Int J Numer Anal Meth Geomech 2000;24:219–43.
[36] Lu N. A semianalytical method of path line computation for transient finite-difference groundwater flow models. Water Resour Res 1994;30:2449–59.
[37] McDonald MG, Harbaugh AW. A modular three-dimensional finite-difference ground-water flow model. US Geological Survey Techniques of Water-Resources Investigations, Book 6, Chapter A1, 1988.
[38] Morton KW, Priestley A, Süli E. Stability of the Lagrange–Galerkin method with non-exact integration. M^2AN 1988;22:625–53.
[39] Pironneau O. On the transport-diffusion algorithm and its application to the Navier–Stokes equations. Numer Math 1982;38:309–32.
[40] Pollock DW. Semianalytical computation of path lines for finite-difference models. Ground Water 1988;26:743–50.
[41] Qin G, Wang H, Ewing RE, Espedal MS. Numerical simulation of compositional fluid flow in porous media, numerical treatment of multiphase flows in porous media. In: Chen Z, et al., editors. Lecture Notes in Physics, vol. 552. Heidelberg: Springer-Verlag; 2000. p. 232–43.
[42] Raviart PA, Thomas JM. A mixed finite element method for 2nd order elliptic problems, mathematical aspects of finite element methods. In: Galligan I, Magenes E, editors. Lecture Notes in Mathematics, vol. 606. Springer-Verlag; 1977. p. 292–315.
[43] Roache PJ. A flux-based modified method of characteristics. Int J Numer Meth Fluids 1992;15:1259–75.
[44] Rudolph DL, Kachanoski RG, Celia MA, LeBlanc DR, Stevens JH. Infiltration and solute transport experiments in unsaturated sand and gravel, Cape Cod, Massachusetts: experimental design and overview of results. Water Resour Res 1996;32:519–32.
[45] Russell TF. Eulerian–Lagrangian localized adjoint methods for advection-dominated problems, numerical analysis 1989. In: Griffiths DF, Watson GA, editors. Pitman Research Notes in Mathematics Series, vol. 228. Harlow, UK: Longman Scientific & Technical; 1990. p. 206–28.
[46] Russell TF, Healy RW. Analytical tracking along streamlines in temporally linear Raviart–Thomas velocity fields. In: Bentley L, et al., editors. Computational Methods in Water Resources, vol. 2. Rotterdam: A.A. Balkema; 2000. p. 631–8.
[47] Russell TF, Heberton CI, Konikow LF, Hornberger GZ. Solving the three-dimensional solute-transport equation using a finite-volume Eulerian–Lagrangian localized adjoint method (FVEL-LAM). In: Seo S, et al., editors. MODFLOW 2001 and Other Modeling Odysseys, Proceedings, vol. 2. International Ground Water Modeling Center, Golden, CO, 2001. p. 497–503.
[48] Russell TF, Trujillo RV. Eulerian–Lagrangian localized adjoint methods with variable coefficients in multiple dimensions, computational methods in surface hydrology. In: Gambolati G, et al., editors. Proc. 8th Int. Conf. on Computational Methods in Water Resources. Southampton, UK: Computational Mechanics Publications; 1990. p. 357–63.
[49] Våg JE, Wang H, Dahle HK. Eulerian–Lagrangian localized adjoint methods for systems of nonlinear advection–diffusion–reaction equations. Adv Water Resour 1996;19:297–315.
[50] Wang H. A family of ELLAM schemes for advection–diffusion–reaction equations and their convergence analyses. Numer Meth PDE 1998;14:739–80.
[51] Wang H. An optimal-order error estimate for an ELLAM scheme for two-dimensional linear advection–diffusion equations. SIAM J Numer Anal 2000;37:1338–68.
[52] Wang H, Al-Lawatia M. An Eulerian–Lagrangian substructuring domain decomposition method for unsteady-state advection–diffusion equations. Numer Meth PDE 2001;17:565–83.
[53] Wang H, Al-Lawatia M, Sharpley RC. A characteristic domain decomposition and space-time local refinement method for first-order linear hyperbolic equations with interfaces. Numer Meth PDE 1999;15:1–28.
[54] Wang H, Al-Lawatia M, Telyakovskiy AS. Runge–Kutta characteristic methods for first-order linear hyperbolic equations. Numer Meth PDE 1997;13:617–61.
[55] Wang H, Dahle HK, Ewing RE, Espedal MS, Sharpley RC, Man S. An ELLAM scheme for advection–diffusion in two dimensions. SIAM J Sci Comput 1999;20:2160–94.
[56] Wang H, Dahle HK, Ewing RE, Lin T, Våg JE. ELLAM-based domain decomposition and local refinement methods for advection–diffusion equations with interfaces. In: Keyes, Xu, editors. Contemporary Mathematics, vol. 180. American Mathematical Society; 1994. p. 361–6.
[57] Wang H, Ersland BG. A characteristic domain decomposition algorithm for two-phase flows with interfaces. In: Bjørstad et al., editors. Ninth International Conference on Domain Decomposition Methods. Bergen, Norway: Domain Decomposition Press; 1998. p. 835–42.
[58] Wang H, Ewing RE. Optimal-order convergence rates for Eulerian–Lagrangian localized adjoint methods for reactive transport and contamination in groundwater. Numer Meth PDE 1995;11:1–31.
[59] Wang H, Ewing RE, Celia MA. Eulerian–Lagrangian localized adjoint methods for reactive transport with biodegradation. Numer Meth PDE 1995;11:229–54.
[60] Wang H, Ewing RE, Qin G, Lyons SL, Al-Lawatia M, Man S. A family of Eulerian–Lagrangian localized adjoint methods for multi-dimensional advection–reaction equations. J Comp Phys 1999;152:120–63.
[61] Wang H, Ewing RE, Russell TF. Eulerian–Lagrangian localized adjoint methods for convection–diffusion equations and their convergence analysis. IMA J Numer Anal 1995;15:405–59.
[62] Wang H, Liang D, Ewing RE, Lyons SL, Qin G. An approximation to miscible fluid flows in porous media with point sources and sinks by an Eulerian–Lagrangian localized adjoint method and mixed finite element methods. SIAM J Sci Comput 2000;22:561–81.
[63] Wang H, Liang D, Ewing RE, Lyons SL, Qin G. An ELLAM-MFEM solution technique for compressible fluid flows in porous media with point sources and sinks. J Comp Phys 2000;159:344–76.
[64] Wang H, Lin T. Solving advection–diffusion equations with interfaces by an Eulerian–Lagrangian localized adjoint method. In: Wang, editors. Advances in Hydro-Science and Engineering, vol. 1(A). University of Mississippi Press; 1993. p. 373–8.
[65] Wang H, Liu J. Development of CFL-free, explicit schemes for multidimensional advection–reaction equations. SIAM J Sci Comput 2001;23:1417–37.
[66] Wang H, Sharpley RC, Man S. An ELLAM scheme for advection–diffusion equations in multi-dimensions. In: Aldama A, et al., editors. Computational Methods in Water Resources XI, vol. 2. Southampton, UK: Computational Mechanics Publications; 1996. p. 99–106.
[67] Wang H, Shi X, Ewing RE. An ELLAM scheme for multidimensional advection–reaction equations and its optimal-order error estimate. SIAM J Numer Anal 2001;38:1846–85.